



OPEN

CDX2 loss in colorectal cancer cells is associated with invasive properties and tumor budding

Nils Bodmer^{1,2,11}, Kristin Uth^{1,2,11}, Rina Mehmeti^{1,2,11}, Cansaran Saygili Demir^{1,10}, Deborah Stroka^{3,4}, Nassim Ghaffari-Tabrizi-Wizsy⁵, Alessandro Lugli¹, Olivier de Wever^{6,7}, Inti Zlobec^{1,8}✉ & Mario P. Tschan^{1,2,9}✉

In colorectal cancer (CRC), tumor buds (TB) are observed histologically as single tumor cell or small tumor cell clusters located mainly at the advancing tumor edge. TB are a marker of poor prognosis and correlate with metastatic disease in CRC patients. They often lack expression of CDX2 and overexpress markers involved in epithelial-mesenchymal transition (EMT). We evaluated the function of CDX2 in CRC proliferation and migration using CRISPR/Cas9 technology and demonstrated a possible link to tumor dissociation and tumor budding. Knocking out CDX2 in CRC cell lines significantly increased migration. Importantly, the observed phenotypes could be rescued by re-expressing CDX2 and by specific CRISPR synergistic activation mediator (SAM) of endogenous CDX2 in CDX2 low expressing CRC cell lines. Multiplex immunofluorescence (mIF) analysis of primary tumor regions compared to TB in a CDX2-positive CRC patient sample as well as patient derived xenografts (PDX) revealed significantly lower CDX2 expression and correlating E-cadherin levels in TB compared to primary tumor regions, in both models. Accordingly, increased invasiveness of CRC CDX2 knockout cells was seen in *ex ovo* xenografts. Taken together, our results provide further insight into the function of CDX2 in preventing CRC cell migration, tumor budding and tumor aggressiveness.

Keywords Colorectal cancer, CDX2, Tumor budding, Cell migration, EMT

Colorectal cancer (CRC) is reported to be the third most common, and the second deadliest cancer worldwide according to statistics by the World Health Organization¹. The main metastatic site remains the liver due to the rich blood supply system that connects both organs. The homeobox protein CDX2 has gained considerable attention over the last years as a potential prognostic biomarker of poor outcome in patients with CRC². Although typically expressed in gastrointestinal tumors, up to 20% of colorectal cancers show a reduction or complete absence of CDX2 protein expression, as detected by immunohistochemistry³. These findings are of clinical relevance, as it has been suggested that patients with stage II CRC (i.e. lymph node metastasis negative) with CDX2 loss represent a particular high-risk group that may benefit from adjuvant therapies⁴.

The mechanism by which CDX2 is lost has not been fully elucidated. Interestingly, the mutation rate of CDX2 is reported to be exceedingly low⁵. On the other hand, DNA promoter methylation and histone acetylation have been described as important epigenetic mechanisms of transcriptional repression and loss of CDX2 protein^{6,7}. CDX2 loss is often seen in cases of chromosomal instability and is expressed in a more heterogeneous manner throughout the tumor tissue. In fact, closer examination of CDX2 staining shows that cells at the invasion front (advancing edge) of the cancer often lose expression².

¹Institute of Tissue Medicine and Pathology, University of Bern, Murtenstrasse 31, 3008 Bern, Switzerland.

²Graduate School for Cellular and Biomedical Sciences, University of Bern, Uni Mittelstrasse, Mittelstrasse 43, 3012 Bern, Switzerland. ³Department of Visceral Surgery and Medicine, Inselspital, Bern University Hospital, University of Bern, Bern, Switzerland. ⁴Department for BioMedical Research, University of Bern, Bern, Switzerland. ⁵Division of Immunology, Research Unit CAM Lab, Otto Loewi Research Center, Medical University of Graz, Graz, Austria.

⁶Cancer Research Institute Ghent (CRIG), Ghent University, Ghent, Belgium. ⁷Laboratory for Experimental Cancer Research, Ghent University, Ghent, Belgium. ⁸Institute of Tissue Medicine and Pathology, University of Bern, Murtenstrasse 31, Room L310, CH-3008 Bern, Switzerland. ⁹Institute of Tissue Medicine and Pathology, University of Bern, Murtenstrasse 31, Room L523, CH-3008 Bern, Switzerland. ¹⁰Lunaphore Technologies, Tolochenaz, Switzerland. ¹¹Nils Bodmer, Kristin Uth and Rina Mehmeti have contributed equally to this work. ✉email: inti.zlobec@unibe.ch; mario.tschan@unibe.ch

Tumor buds are defined as single tumor cells or small tumor cell clusters of up to four cells detached from the main tumor body on histological sections⁸. Over the last decade, the process of “tumor budding” has gained tremendous attention due to its consistent and reproducible unfavorable prognostic effect^{9,10}. In fact, in 2016, the International Tumor Budding Consensus Conference (ITBCC) took place to reach a consensus on tumor bud scoring and reporting as well as to establish the clinical scenarios under which budding plays a relevant role in CRC management⁸. Tumor budding occurs in a multitude of different cancer types, e.g. lung, head and neck, pancreas, and breast cancer, thus has far reaching clinical importance^{11–14}.

Tumor buds are associated with loss of the cell-to-cell adhesion molecule E-cadherin, leading to translocation of β -catenin to the nucleus, and upregulation of numerous proteins involved in extracellular matrix degradation as well as invasion and migration of tumor cells^{15,16}. In fact, co-expression of epithelial and mesenchymal markers in a subset of tumor buds speaks for a partial EMT state in these cells¹⁷.

We hypothesize that downregulation of CDX2 promotes colorectal cancer cell migration, invasion and tumor budding predisposing patients to poor prognosis and therapy response due to increased metastasis. We aim to elucidate the future potential of CDX2 as a therapeutic target to counteract CRC cell dissemination in patients.

Results and discussion

Loss of CDX2 increases migration and invasion of colorectal cancer cells

To investigate whether CDX2 loss can impact CRC proliferation and migration *in vitro*, we generated LS174T and CaCo2 CDX2 knockout cells^{18,19}. We transduced these cell lines with two lentiviral CRISPR/Cas9 constructs encoding two independent gRNAs targeting exon 1 of the *CDX2* gene. Expression of both gRNAs resulted in *CDX2* knockout phenotypes in all colon cancer cell clones (Fig. 1a, e; Supp. Fig. S1a, b).

To test how CDX2 affects cellular proliferation, we performed cell counting and colony formation assays with control and *CDX2* knockout CRC cells. Our results revealed significantly lower cell numbers of CaCo2 and LS174T *CDX2* knockout cells in comparison to the parental cells after 4 days in culture (Suppl. Fig. S1c, f) in alignment with reduced colony formation (Suppl. Fig. S1d, e, g, h). Since knocking out *CDX2* did not cause increased cell proliferation, we analyzed the migratory potential of these *CDX2* knockout cell lines using wound healing and transwell migration and invasion assays. We found significantly increased migratory ability of CaCo2 *CDX2* knockout cell clones in comparison to parental tracking the migration of the cells by live cell imaging (Fig. 1b). Since the growth behavior of LS174T cells did not allow to generate a well-defined scratch in a cell monolayer, we performed transwell migration assays with these cells and analyzed the migration rate through the porous membrane of the insert. Similar to CaCo2 *CDX2* knockout cells, LS174T *CDX2* knockout clones showed significantly increased migratory activity compared to their respective control clones (Fig. 1f). In addition, knocking out *CDX2* significantly increased cellular invasion in matrigel (Fig. 1g).

To investigate whether the observed increased motility phenotype is specifically due to *CDX2* modulation we performed an add-back experiment in CaCo2 *CDX2* knockout cells. We overexpressed *CDX2* in CaCo2 *CDX2* knockout cells using a lentiviral construct encoding for FLAG-tagged human *CDX2* (Fig. 1a; Suppl. Fig. S1a). Firstly, re-expressing *CDX2* restored the proliferation rate as found in the CaCo2 wildtype cells (Suppl. Fig. S1i). Secondly, the migratory potential assessed in wound healing and transwell migration was reversed to near-wildtype levels in *CDX2*-rescued CaCo2 cells (Fig. 1b, c). Thirdly, re-expressing *CDX2* also reversed the increased invasion rate caused by *CDX2* depletion (Fig. 1d).

At first glance, the above data of decreased proliferation versus increased cell motility in *CDX2* CRC knockout cells seem in contrast to previous findings demonstrating that knocking down *CDX2* leads to increased proliferation in CaCo2 and HT29 colon cancer cells¹⁹. This discrepancy might be based on using *CDX2* null instead of knockdown cells where residual *CDX2* might be responsible for a contradictory phenotype. This discrepancy could also be caused by hypoxic conditions¹⁹. Strikingly, our results showed a significant increase in the migration and invasion ability of *CDX2* knockout in two different CRC cell lines. These results indicate that loss of *CDX2* expression indeed promotes a more aggressive cancer phenotype, consistent with the existing literature on the well-documented correlation of *CDX2* loss with unfavorable patient outcome^{4,21}. Our findings are in agreement with previously published data showing that *CDX2* has a negative effect on colon cancer motility and dissemination²². Consequently, *CDX2* likely is an important modulator of colorectal cancer progression.

Specific (re-)activation of endogenous *CDX2* in *CDX2* negative colorectal cancer cells resulted in decreased cell motility

To further validate our findings from *CDX2* knockout and overexpression experiments in a more physiologically relevant model, we activated endogenous *CDX2* in *CDX2* negative SW620 and HT29 colon cancer cell lines. To this end we designed several gRNAs targeting the proximal 5'UTR region of *CDX2* and transduced them together with the lentiviral CRISPR/dCas9 Synergistic Activation Mediator (SAM) and the helper activator complex, MS2-p65-HSF1 into SW620 and HT29 cells (Fig. 2a). Two of the gRNAs tested allowed for activation of endogenous *CDX2* expression in SW620 and HT29 cells as shown by western blotting and immunohistochemistry (Fig. 2b, d; Suppl. Fig. S2a). Activation of endogenous *CDX2* in SW620 cells resulted in an increase of cellular proliferation and colony formation (Suppl. Fig. S2b, c, d) supporting our previous *CDX2* knockout data in CRC cells showing decreased proliferation and colony formation upon gene knockout. Importantly, activation of endogenous *CDX2* expression mediated by the CRISPR/SAM system significantly attenuated transwell migration in both CRC cell lines. The effect of transwell migration attenuation was *CDX2* dose dependent, which varied between the two different gRNAs and the two cell lines (Fig. 2c, e). Further, the assessment of transwell invasion in HT29-SAM cells showed a similar pattern upon *CDX2* activation and thus supports our findings from above analysis (Fig. 2f).

As hypothesized, activation of endogenous *CDX2* expression using a CRISPR/dCas9 synergistic activation mediator (SAM) system allowed of specific activation of *CDX2*²³ paralleled by a decrease in cell migration as well

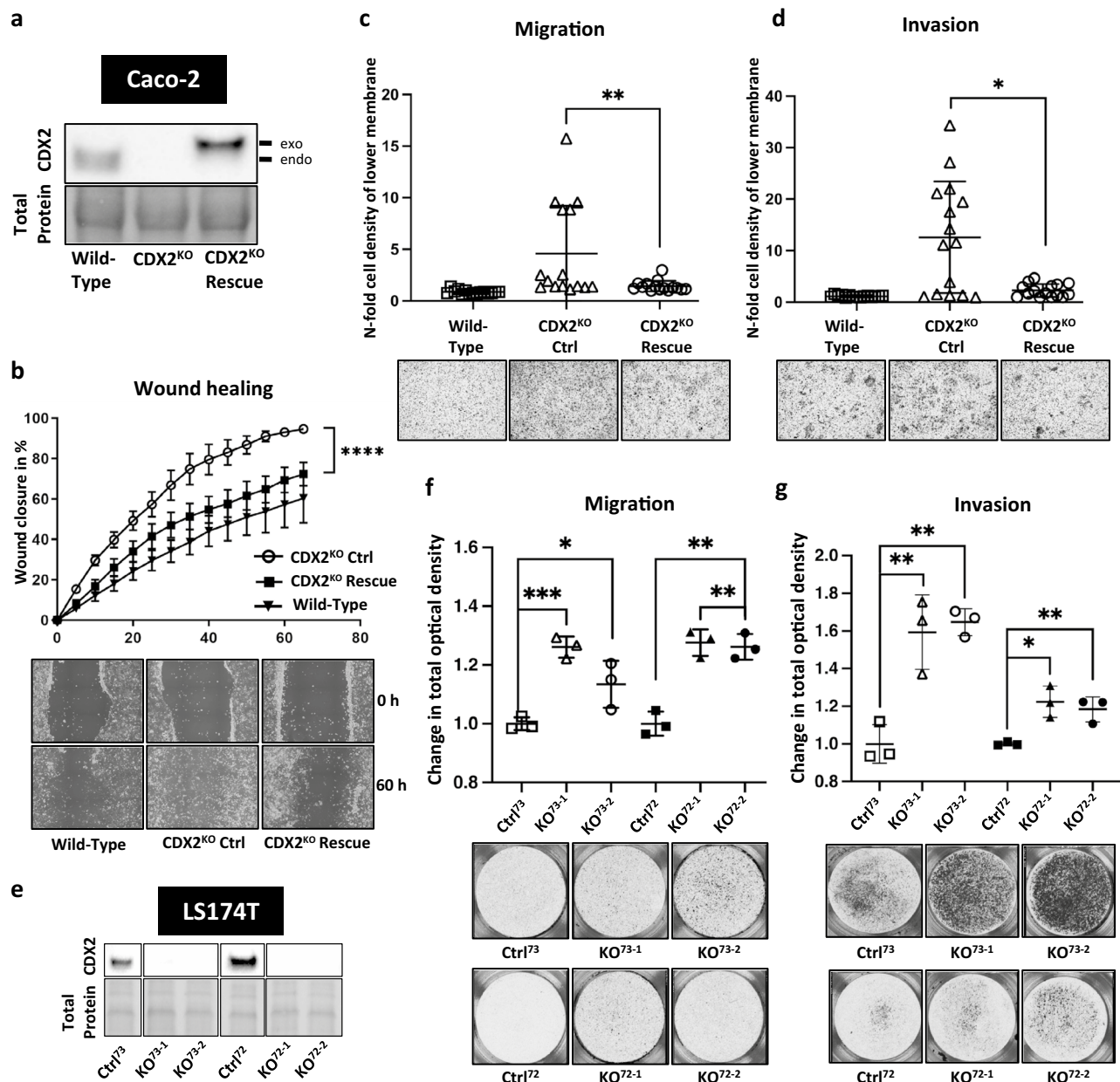


Fig. 1. Deletion of CDX2 in colorectal cancer (CRC) cells promotes cancer cell migration and its exogenous expression in Caco-2 CDX2 knockout cells is able to rescue this phenotype. (a) Western blot analysis confirming CDX2 knockout and rescued Flag-CDX2 in Caco-2 cells (endo = endogenous, exo = exogenous). (b) Wound healing assay of CDX2 rescued compared to CDX2 knockout cells as control (mean + SEM). (c) Transwell migration assay of cells in (a). (d) Transwell invasion assay of cells in (a). Statistical evaluation using two-way ANOVA and nonparametric Mann-Whitney U were applied for wound healing and transwell migration/invasion assays, respectively, on PRISM software (GraphPad Software, San Diego). (e) Western blot confirming CDX2 deletion in four LS174T CDX2 knockout clones (KO⁷³⁻¹, KO⁷³⁻², KO⁷²⁻¹, KO⁷²⁻²) compared to two controls (Ctrl⁷³, Ctrl⁷²) (relevant sections of the whole blot). (f) Transwell migration assay of cells in (e). (g) Transwell invasion assay of cells in (e). Statistical evaluation using two-way ANOVA and unpaired T-test was done for wound healing and transwell migration/invasion assays, respectively, on PRISM software (GraphPad Software, San Diego). $n \geq 3$. * $p \leq 0.05$; ** $p \leq 0.01$; *** $p \leq 0.001$; **** $p \leq 0.0001$ in all graphs.

as invasion^{19,21}. Of note, CDX2 reduces cellular motility in a dose-dependent manner that is in line with previous findings from our group that showed dose-dependent epigenetic silencing of CDX2 and thus supporting a quantitative relevance⁷. Together, reactivation of CDX2 expression in CDX2-negative colorectal cancer reduces tumor cell migration and invasion¹⁹.

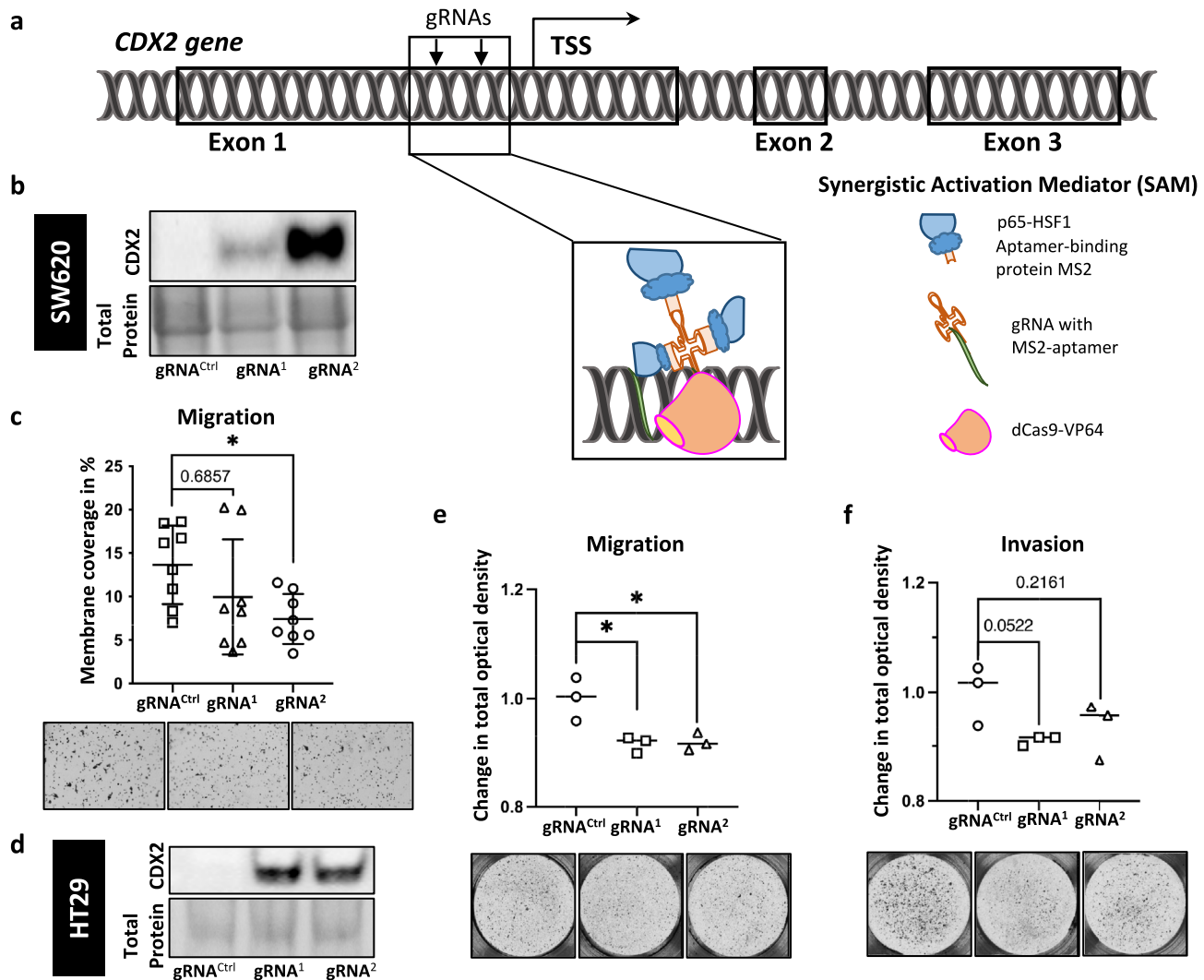


Fig. 2. Endogenous CDX2 activation in SW620 and HT29 cell lines causes significant decrease of cell motility. (a) Schematic representation of the CRISPR/dCas9 SAM system in SW620 and HT29 colon cancer cell lines. Two gRNAs bind the MS2 aptamer attached to p65-HSF1 (enhancer of transcriptional activation) and guide dead (d) Cas9 to CDX2 promoter regions upstream of the transcriptional start site (TSS). (b) Western blot confirmation of CDX2 protein expression in SW620 cells. (c) Transwell migration assay of SW620 cells in (b), $n > 3$. (d) Western blot confirmation of CDX2 protein expression in HT29 cells. (e) Transwell migration assay of HT29 cells in (d), $n = 3$ in (e) and (f). Nonparametric Mann–Whitney U was applied for transwell migration assay with $n > 3$, whereas unpaired T-test was applied for transwell migration and invasion assay with $n = 3$, on PRISM software (GraphPad Software, San Diego). * $p \leq 0.05$.

Low CDX2 and E-Cadherin expression levels are associated with tumor budding at the primary site and at the liver metastatic site of CRC patients

By applying multiplex immunofluorescence on CRC patient and patient-derived xenograft (PDX) samples, we were able to explore an association between low CDX2 and E-cadherin levels, the latter being a well-established EMT marker, in tumor buds and corresponding nearest tumor region (Fig. 3a-f). Quantitative analysis showed that both CDX2 and E-cadherin levels were significantly lower in tumor buds compared to their adjacent tumor regions in a CRC patient sample (Fig. 3c). Interestingly, in the PDX model, representing metastasis of CRC in the liver, we were able to identify tumor buds as well. Similarly to the primary CRC sample, we observed significantly lower CDX2 and E-cadherin levels in tumor buds compared to the cells in the nearest tumor region (Fig. 3f). In line with these findings *in vivo*, we also observed significantly reduced mRNA and protein levels of E-Cadherin in LS174T CDX2 knockout compared to wild-type cells *in vitro* (Suppl. Fig. S3a, b, c).

These findings suggest that downregulation of CDX2 is a predisposition for detached and disseminated CRC cells from the main tumor, such as tumor buds. Tumor budding has been described as an independent prognostic factor and associated with lymph node metastasis in CRC⁸. Previous studies have also linked decreased CDX2 expression to a more aggressive phenotype and poorer prognosis in CRC^{22,23}. Additionally, the decrease in

E-cadherin levels suggests an ongoing epithelial-mesenchymal transition (EMT) process within tumor buds, which may contribute to their invasive properties. Moreover, CDX2 has also been described as an inhibitor of EMT²⁴. However, these findings are limited by the sample size and the reliance on immunocompromised mice for the PDX model, which may not fully recapitulate human tumor microenvironment. Nevertheless, this proof-of-concept analysis demonstrated the feasibility of using multiplex immunofluorescence in analyzing expression of multiple markers in tumor buds, laying the groundwork for broader application in larger cohorts. Future studies should also explore the mechanisms by which CDX2 modulates EMT and tumor budding. Such studies may provide valuable insights into the development of selective therapies targeting tumor bud formation and inhibiting CRC metastasis.

Increased invasive behavior of CDX2 knockout cells *ex ovo*

To further test our hypothesis that loss of CDX2 contributes to a more aggressive behavior of colorectal cancer cell lines, we made use of the chorioallantoic membrane assay (CAM)^{18,19}. The chorioallantois of the chicken egg provides a physiological environment for the colorectal cancer cells to grow and thus represents a relevant tool to study the behavior of colorectal cancer cells²⁵. The application of LS174T CDX2 knock-out clones (Fig. 3g-l) onto the chicken egg revealed substantial differences in aggressiveness to its relative control clone (Ctrl73). LS174T cells showed a strongly increased tissue infiltration in one CDX2 knockout clone compared to control cells (Fig. 3g). Additionally, we were able to detect tumor budding (TB) in the tissue slides created from CAM assay cell grafts (Fig. 3l). Tumor budding count suggested an increased frequency for clone KO73-2 compared to control (Fig. 3h). In summary, depleting CDX2 in CRC cells increased their aggressive phenotype in a xenograft model.

3D models show that loss of CDX2 expression is a key feature of enhanced invasive tumor cells^{9,24}. In patient samples as well as in the 3D models, invasive cells show a significant reduction of CDX2 expression and epithelial cell markers such as E-cadherin¹³. These results suggest a transformation of cells with epithelial characteristics to mesenchymal-like cells, which then are able to penetrate tissue as first step towards the formation of metastases. Our findings are supported by the observation that CDX2 expression and cell polarization is lost in the tumor buds but restored in the resulting metastasis²⁶. Further, we showed that the CAM assay provides an opportunity to model tumor budding for colorectal cancer cells²⁵. The CAM assay is, compared to *in vivo* animal models, a more simplistic, rapid, resource-saving model that can be used as a valuable preliminary step prior to more complex animal models²⁵. Further studies are needed to elucidate the role of CDX2 in preventing an EMT-like phenotype which is closely related to tumor budding and associated with an increased risk for colorectal cancer patients^{7,20,24}.

We provided further evidence of a key role of CDX2 in preventing tumor cell dissemination and possibly tumor budding using state-of-the-art CRISPR/Cas9 and /dCas9 technology to manipulate CDX2 expression in colon cancer cells. We also showed that loss of CDX2 is associated with tumor budding and leads to a more aggressive phenotype in several 3D models. Additionally, the newly generated cell models will facilitate more physiological relevant studies in the future, aiming at deciphering the function of CDX2 in colon cancer pathology. In conclusion, our data hint to a substantial role of CDX2 in tumor progression in 2D and 3D models, which should be further investigated.

Materials and methods

Cell culture

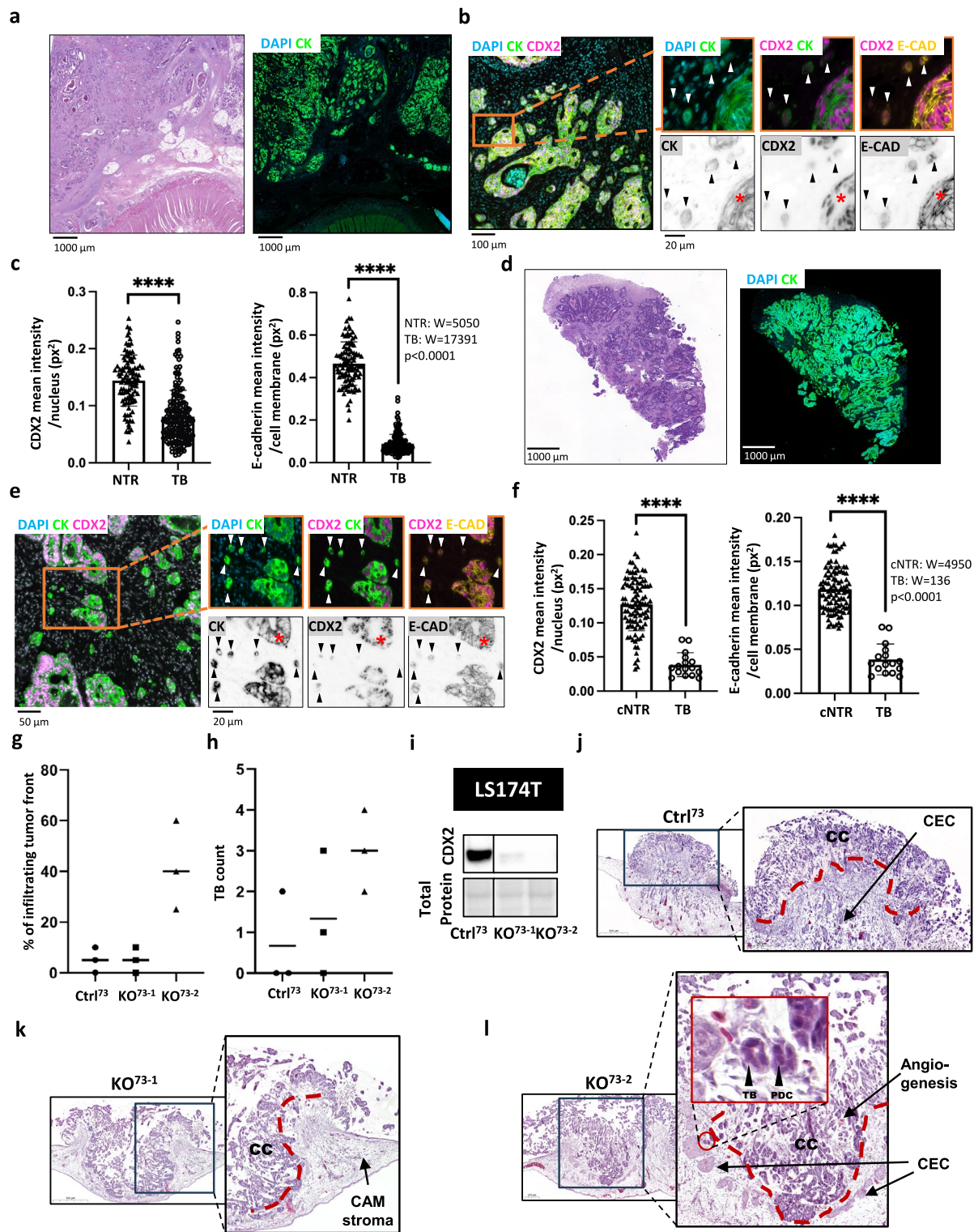
LS174T (ATCC) cells were maintained in Dulbecco's Modified Eagle's Medium (DMEM, D6046, Sigma) supplemented with 10% Fetal Bovine Serum (FBS, Sigma) and 2 mM L-Glutamine (G7513, Sigma). CaCo2 (ATCC) cells were grown in Minimum Essential Medium Eagle (EMEM, M4526, Sigma) supplemented with 20% FBS and 2 mM L-Glutamine and SW480 and SW620 (ATCC) cells were kept in RPMI-1640 (RPMI, R8758, Sigma) supplemented with 10% FBS. HT29 were kept in Mc Coy's 5A (M8403, Sigma) supplemented with 10% FBS and 2 mM L-Glutamine. All cells were cultured in a humidified atmosphere of 5% CO₂.

Lentiviral vectors

CRISPR-Cas9 *CDX2* *knockout* two gRNA sequences (HGLibA_08899: CTACGGCGGTTACCACGTGG and HGLibA_08898: GACTGGAATGGCTACGCGCC) targeting the *CDX2* gene were taken from the Human GeCKOv2 CRISPR knockout pooled library and cloned into the lentiCRISPR v2 vector (kindly provided by Feng Zhang, Addgene plasmid #52,961) using In-Fusion[®] Cloning (Takara Bio USA, Inc.) according to their instructions.

CDX2 *expression vector* Human *CDX2* cDNA was amplified from the CMV-*CDX2*-WT plasmid kindly provided by Bert Vogelstein (Addgene plasmid #16,553). We added a Flag-sequence to the forward primer for tagging *CDX2* and cloned the Flag-*CDX2* fragment into pLV-EF1a-IRES_Neo backbone kindly provided by Tobias Meyer (Addgene plasmid #85,139) using In-Fusion[®] Cloning (Takara Bio USA, Inc.) according to their instructions.

Synergistic Activation Mediator (SAM) system vectors The following SAM system lentiviral plasmids were a gift from Feng Zhang: lenti-sgRNA-(MS2)_zeo backbone (Addgene plasmid #61,427), lenti-dCAS9-VP64_Blast (Addgene plasmid #61,425), and lentiMPH_v2 (Addgene plasmid #89,308). Four different gRNAs were designed using the Cas-Activator-Tool (<http://sam.genome-engineering.org/database>) and cloned into the lenti-sgRNA-(MS2)_zeo backbone. Two of the four *CDX2* gRNA sequences (AGGGGAGGGAGGGCTCGTGAG and GAGGAAGCTCTTAACAATAA) resulted in marked activation of endogenous *CDX2* expression. We used a control gRNA cloned in the same (MS2) zeo backbone as negative control.



Lentiviral vector preparation and cell transduction

293T cells for virus production were maintained in DMEM (Sigma-Aldrich, St. Louis, MO, USA), supplemented with 5% FBS, 1% penicillin/streptomycin (Sigma-Aldrich), and 1% Hepes (Sigma-Aldrich), and kept in 7.5% CO₂ at 37 °C.

The following lentiviral vectors CRISPR-Cas9-CDX2-gRNA1 (HGLibA_08899), CRISPR-Cas9-CDX2-gRNA2 (HGLibA_08898) (Zhang lab), and pCas-Scramble CRISPR Vector (Cat#: GE100003, Origene) contained a puromycin antibiotic-resistance gene for selection of transduced mammalian cells. The Flag-CDX2 expression vector contained a hygromycin antibiotic-resistance gene for selection of transduced mammalian cells.

Lentiviral vectors for the SAM system, namely lenti-sgRNA-(MS2)_zeo, lenti-dCas-VP64_Blast and lentiMPH_v2 contain a zeocin, blasticidin and hygromycin antibiotic-resistance gene, respectively, for selection of transduced mammalian cells.

◀ **Fig. 3.** CDX2 and E-cadherin expression in tumor buds versus primary tumor in a CRC patient sample. (a, d) H&E staining of the whole slide image of a CRC patient sample and patient-derived xenograft (PDX) model, respectively. (b, e). The panels illustrate downregulation of cytokeratin (CK), CDX2 and E-cadherin (E-CAD) in tumor buds (indicated by arrowheads) compared to the nearest primary tumor regions (indicated by asterix). (c, f) Graphs show CDX2 and E-cadherin expression quantified in tumor buds versus epithelial cells in the nearest tumor region. (c) NTR, nearest tumor region n = 100, TB, tumor buds n = 186, *** $p < 0.0001$. (f) cNTR, cells in the nearest tumor region n = 99, TB, tumor buds n = 16, *** $p < 0.0001$. Wilcoxon signed-rank test was applied for statistical evaluation on PRISM software (GraphPad Software, San Diego). (g–l) Chorioallantoic membrane (CAM) assay of LS174T CDX2 knockout clones vs. CDX2 positive control. (g) Infiltrating margin analysis and (h) tumor bud count of cells incubated on CAM, stained for H&E. (i) Western blot confirmation of CDX2 knockout of cells used for CAM assay. (j–l) CAM tissue slides stained for H&E of one control (Ctrl⁷³) and two CDX2 knockout clones (KO⁷³⁻¹ and KO⁷³⁻²); CEC: CAM epithelial cluster; CC: Cancer cells; TB: Tumor bud; PDC: poorly differentiated cluster.

Third generation lentiviral particles were produced by transient co-transfection of the packaging plasmids pMD.G (VSV-G), pMDLg/p.RRE (gag and pol), and pRSV-Rev (Rev gene), as well as the respective lentiviral transfer vector. Viral supernatant was harvested 48 h later. Cell lines were seeded in 6-well plates one day before the transduction was performed overnight using 500 μ L viral supernatant and 8 μ g/ml polybrene per well. Four days after transduction the cells were selected with the respective antibiotics (Puromycin, 1.5 μ g/ml; Hygromycin, 100–600 μ g/ml; Blasticidin, 5 μ g/ml; Zeocin, 200–1000 μ g/ml). Where necessary single cell cloning was performed by serial dilution of cells in 96-well plate format.

Western blot analysis

Cell lysates were prepared using 8 mM Urea in ELGA® water containing TBS-T and 0.5% (v/v) Triton X-100 supplemented with Protease Inhibitor (04,693,116,001; Roche Diagnostics, Rotkreuz, Switzerland). Protein concentrations were determined using a Bradford Assay (Bio-Rad Protein Assay; Bio-Rad, Cressier, Switzerland). 30–50 μ g of total protein was mixed with loading buffer (4 \times Laemmli Sample Buffer, Cat: #161–0747, BioRad) to a total volume of 15 μ l, loaded on Mini-Protean TGX Stain Free Gels (12%, 15-well, Cat. #456–8095; BioRad) and transferred to a PVDF membrane (0.2 μ m PVDF, Cat. #170–4156; BioRad) using a Trans-Blot Turbo Transfer Pack (Mini format; BioRad). Membranes were blocked with 5% milk in 1X Tris buffered Saline with 0.1% Tween® (TBS-T) for at least 30 min. Blots were incubated with anti-CDX2 (1:5000 in 5% BSA in TBS-T; EPR2764Y, Sigma-Aldrich) and anti-E-Cadherin (1:1000 in 5% milk in TBS-T; 14,472, Cell Signaling) over night at 4 °C followed by incubation with anti-rabbit or anti-mouse, respectively (1:10'000 in BSA; Cell Signalling Technology, Leiden, The Netherlands) for at least one hour at RT. Detection has been performed using ECL substrate (Clarity Western ECL Substrate, Cat. #170–5060; BioRad) and a ChemiDoc system (#731BR00765; BioRad). To quantify western results, protein expression was normalized to total protein expression using ImageJ software version 1.54d (www.imagej.net/ij/).

Cell growth and colony formation assays

For trypan blue counting 4×10^4 cells were seeded in duplicates in a 24-well plate and were counted every day using Neubauer chambers (Neubauer). For colony formation assays SW620 and LS174T cells were seeded in 6-well plates at a density of 1×10^3 cells per well. CaCo2 cells were seeded at a density of 0.5×10^3 cells per well. After 6 (SW620, CaCo2) or 10 days (LS174T) cell colonies have been fixed with 4% sterile-filtered PFA for 15 min and stained with 0.05% Crystal Violet (V5265, Sigma) in 30% EtOH for one hour. Plates have been washed two times with PBS, once with distilled water, then dried overnight. Colonies were counted using an Oxford Optronix Gelcount TM apparatus (Oxford Optronix, UK).

Wound-healing assays

Wound healing: CaCo2 cells and the respective sublines were seeded in duplicates in 6-well plates (Sarstedt) at a density of 9.5×10^5 /well. After 24 h a scratch was applied across the well using a pipette tip. Live cell imaging was performed on a Cell IQ2 cell imaging and analysis system (110,004; Chip-Man Technologies). Wound closure was determined using CellActivision software (Yokogawa Electric Corporation, www.yokogawa.com).

Transwell migration/invasion assays

Transwell migration assay: The respective cells were seeded in 0%FBS Media one day prior to experiment at 2×10^6 cells in a 10 cm dish. SW620, LS174T, HT29-SAM and CaCo2 cells were seeded at densities of 4×10^5 , 2×10^5 , 2×10^5 and 5×10^4 cells per transwell insert (TC for 24well, PET 8 μ m, Sarstedt) in medium without FBS, respectively. Transwell inserts were then placed in a 24-well plate (Sarstedt, Suspension Plates), each well containing medium supplemented with 20% FBS as a chemoattractant for 48 h.

Transwell invasion assay: To assess the invasion capabilities of the following cell lines the transwell inserts were coated with 50 μ L Matrigel (Corning, Cat:5,236,014). CaCo2, LS174T and HT29-SAM cells were subsequently seeded at a density of 1×10^5 , 2×10^5 and 2×10^5 cells per insert, respectively (TC for 24well, PET 8 μ m, Sarstedt). The inserts were placed in an empty 24-well plate and 550 μ l medium were added to the well below. The media was supplemented with 40% FBS (as a chemoattractant) for a 40 h incubation of Caco2 cells and 20% FBS and 48 h for LS174T and HT29 SAM cells.

The chick chorioallantoic membrane (CAM) assay

To perform the *ex ovo* chick chorioallantoic membrane assay (CAM assay) fertile white Lohmann chicken eggs (Schropper, Gloggnitz, Austria) were washed and incubated at 37.6 °C and 40–60% humidity. On day three of embryonic development (EDD3) eggs were carefully cracked and content transferred into sterile weighing boats (100 ml, 85×85×24 mm, VWR®, Avantor, Vienna, Austria) and covered with a sterile quadratic 10×15 mm petri dish (Bartelt, Graz, Austria) and further incubated under the same conditions as mentioned above. On EDD10, sterile silicone rings of 5 mm diameter were placed on the CAM of each embryo, avoiding placement directly on bigger blood vessels. The cells were then added at 1×10⁶ cells in 15 μl Medium plus 5 μl Matrigel® (Corning® Matrigel® Basement Membrane Matrix, Phenol Red-Free, 10 mL, Product #356,237) in the center of each silicone ring. After another 72 h, on EED 13, the formed CAM tumors were photographed, excised and fixed in 4% PFA and paraffin embedded according to standard protocol. Further analysis was done by Haematoxylin/Eosin (H&E) staining and subsequent Immunohistochemistry (IHC). CAM fulfills the 3R principle (Replacement, Refinement and Reduction) by representing an alternative to animal models. The tumor scoring, budding analysis and margin characterization was performed by a trained pathologist based on the H&E slides.

Primary patient sample

One CRC patient sample block was retrieved from the archives of the Institute of Tissue Medicine and Pathology, University of Bern. The corresponding diagnostic H&E slides were evaluated for budding and deemed appropriate for downstream analysis with multiplex immunofluorescence. Informed consent was obtained from the patient prior to surgery.

Patient-derived Xenograft (PDX) models

Human CRC tumor tissues were obtained from consented patients at the University Hospital of Bern undergoing surgical colorectal resection. Informed consent was obtained prior to surgery in compliance with the local ethics regulations and under approval of local ethics commission. All animal experiments were carried out in accordance with relevant guidelines. Tumor samples were taken from within the tumor margin as well as from outside the tumor margin to be used as a non-malignant control. Tumor tissue samples were collected in basic medium. Tumor fragments were transplanted subcutaneously in immunocompromised mice (Rag2/Il2rg double knockout, C57BL/6NTac.Cg-Rag2^{tm1Fwa}Il2rg^{tm1Wjl}, obtained from Taconic Biosciences).

To implant the tumors, mice were anesthetized with 2% isoflurane at a flow rate of 2L/min and simultaneously administered the analgesic buprenorphine (Temgesic™) at a dose of 0.1 mg/kg. The PDX tumor was removed from mice after 1–3 months when the tumor reached a volume of 1,500 mm³ and further processed as previously described²⁷. To explant the tumors, the mice were treated as described above. Tumor tissue and blood were collected, and the animals were sacrificed by exsanguination.

Approval statement

The study involving primary patient samples was approved by the Ethics Committee of the Canton of Bern, Switzerland (2020-00,498). Ethical approval for all animal experiments was also obtained from the Ethics Committee of the Canton of Bern, and the PDX license (BE85/18) was granted by the Veterinary Service (Veterinärerdienst) of the Canton of Bern. The study was conducted in strict accordance with ARRIVE 2.0 guidelines to ensure the ethical and accurate reporting of animal research. All methods were performed in accordance with the relevant guidelines and regulations.

Immunohistochemistry (IHC)

For immunohistochemical (IHC) analysis LS174T, CaCo2, SW620, and SW480 cells were detached using trypsin and washed once with PBS. Cell pellets were formalin-fixed, paraffin embedded (FFPE), cut into 2 μm sections and mounted on glass slides. Before incubation with CDX2 (EPR2764Y, Cell Marque, Sigma-Aldrich) or E-Cadherin (13–17,000, Thermo Fischer Scientific) antibody, the sections were pretreated (HIER=heat induced epitope retrieval) with pH high/ low buffer to unmask the target antigens, counterstain with Haematoxylin. Slides were stained with BOND RX (Leica Biosystems) and scanned with a Pannoramic 250 Flash II (3DHistech Ltd., Budapest, Hungary) scanner.

Sequential immunofluorescence and image acquisition

2.5 μm thick FFPE sections underwent simultaneous dewaxing and antigen retrieval protocol on PT Module™ (Epredia). Tissue sections were placed on the rack of PT module and incubated in the Dewax and HIER Buffer H (TA999-DHBH, Epredia) for 1 h at 102 °C. Subsequently, slides were rinsed and stored in Multistaining Buffer (BU06, Lunaphore Technologies) until use. After this preparation step, the sample, reagents, and buffers were loaded on COMET™ (Lunaphore Technologies).

COMET™ performs sequential immunofluorescence (seqIF™), where tissues undergo subsequent cycles of staining, imaging, and antibody elution in a fully automated manner. Staining is performed with standard unconjugated primary antibodies and secondary antibodies labeled with fluorophores. DAPI (Thermo Scientific) is used as counterstaining reagent. Antibodies are listed in Table 1. Image acquisition step is integrated on the device and after imaging, removal of antibodies is achieved with a gentle elution protocol that prepares tissue for the next staining-imaging cycle. At the end of the assay, a single ome.tif file that contains an already stitched, aligned, and stacked image is ready to visualize all the markers and counterstaining. Background subtraction can be applied by Lunaphore Viewer for the detection of distinct signals.

	Antibody	Supplier	Catalog no	Clone
Primary antibodies	CDX2	Cell Marque	235R-16	EPR2764Y
Secondary antibodies	Cytokeratin	Dako	M3515	AE1/AE3
	E-cadherin	BD Bioscience	610,181	36/E
Secondary antibodies	Alexa Fluor™ Plus 647, goat anti-Rabbit	Lunaphore Technologies	DR647RB	-
	Alexa Fluor™ Plus 647, goat anti-Mouse	Lunaphore Technologies	DR647MS	-
	Alexa Fluor™ Plus 555, goat anti-Mouse	Lunaphore Technologies	DR555RB	-
	Name	Supplier	Catalog no	
Counterstain	DAPI	Thermo Scientific	62,248	

Table 1. List of antibodies.

Digital image analysis

The CRC patient multiplex scan was divided into 100 smaller images of equal size (W: 836.74 μm , H: 837.89 μm). We randomly chose 30 images to analyze tumor buds. Images were analyzed by using open-source software QuPath version 0.3.0 (<https://qupath.github.io/>). DAPI, CDX2, Cytokeratin (CK), and E-cadherin (E-CAD) channels were exported. In QuPath, tumor buds were annotated manually as well as the corresponding nearest primary tumor region. CK was used to facilitate the identification of tumor cells (including tumor buds), i.e. only CK + DAPI + objects were considered. Within these annotated areas, the Stardist algorithm was used for nuclear segmentation based on DAPI (nuclear) staining within QuPath. Additionally, expression measurements for protein markers CDX2, and E-cadherin were acquired. Although CDX2, as a nuclear marker, could be accurately quantified without modification of the Stardist, to correctly estimate E-cadherin (membrane marker) expression adjustments using *cellExpansion* and *cellConstrainScale* were performed. This was done to align the cell segmentation line along the border of the cell for a more accurate measurement of E-cadherin expression level. The same approach was used for the PDX model multiplex scan.

Statistics and data analysis

Statistical analyses were conducted using the PRISM software (GraphPad Software version 10.1.2, San Diego, www.graphpad.com). Nonparametric Mann-Whitney U, for transwell migration and transwell invasion, colony formation and cell count with $n > 3$, unpaired T-test, for transwell migration and transwell invasion with $n = 3$, and two-way Anova, for wound healing assay, were applied. For multiplex data analysis, Wilcoxon signed-rank test was applied to determine differences in expression of CDX2, E-cadherin in tumor buds versus mean CDX2, E-cadherin expression in corresponding, nearest tumor regions, respectively. P values $p < 0.05$ were considered to be statistically significant.

Data availability

The raw data of this study are included in the supplementary material. Further inquiries can be directed to the corresponding authors.

Received: 15 December 2024; Accepted: 13 June 2025

Published online: 06 July 2025

References

1. World Health Organization (WHO) 2023, *World health organization website*, Colorectal cancer, accessed August 2024, <https://www.who.int/news-room/fact-sheets/detail/colorectal-cancer>.
2. Olsen, J., Espersen, M. L., Jess, P., Kirkeby, L. T. & Troelsen, J. T. The clinical perspectives of CDX2 expression in colorectal cancer: A qualitative systematic review. *Surg. Oncol.* **23**(3), 167–176. <https://doi.org/10.1016/j.suronc.2014.07.003> (2014).
3. Lugli, A., Tzankov, A., Zlobec, I. & Terracciano, L. M. Differential diagnostic and functional role of the multi-marker phenotype CDX2/CK20/CK7 in colorectal cancer stratified by mismatch repair status. *Mod. Pathol.* **21**(11), 1403–1412. <https://doi.org/10.1038/modpathol.2008.117> (2008).
4. Dalerba, P., Sahoo, D. & Clarke, M. F. CDX2 as a Prognostic Biomarker in Colon Cancer. *N Engl. J. Med.* **374**(22), 2184. <https://doi.org/10.1056/NEJMcl602584> (2016).
5. Hinoi, T., Loda, M. & Fearon, E. R. Silencing of CDX2 expression in colon cancer via a dominant repression pathway. *J. Biol. Chem.* **278**(45), 44608–44616. <https://doi.org/10.1074/jbc.M307435200> (2003).
6. Wang, Y., Li, Z., Li, W., Liu, S. & Han, B. Methylation of CDX2 gene promoter in the prediction of treatment efficacy in colorectal cancer. *Oncol. Lett.* **16**(1), 195–198. <https://doi.org/10.3892/ol.2018.8670> (2018).
7. Graule, J. et al. CDX2 in colorectal cancer is an independent prognostic factor and regulated by promoter methylation and histone deacetylation in tumors of the serrated pathway. *Clin. Epigenetics* **10**(1), 120. <https://doi.org/10.1186/s13148-018-0548-2> (2018).
8. Lugli, A. et al. Recommendations for reporting tumor budding in colorectal cancer based on the International tumor budding consensus conference (ITBCC) 2016. *Mod. Pathol.* **30**(9), 1299–1311. <https://doi.org/10.1038/modpathol.2017.46> (2017).
9. Cappellosso, R. et al. Tumor budding as a risk factor for nodal metastasis in pT1 colorectal cancers: a meta-analysis. *Hum. Pathol.* **65**, 62–70. <https://doi.org/10.1016/j.humpath.2017.04.013> (2017).
10. Rogers, A. C. et al. Systematic review and meta-analysis of the impact of tumour budding in colorectal cancer. *Br. J. Cancer* **115**(7), 831–840. <https://doi.org/10.1038/bjc.2016.274> (2016).
11. Kadota, K. et al. Tumor budding correlates with the protumor immune microenvironment and is an independent prognostic factor for recurrence of stage I lung adenocarcinoma. *Chest* **148**(3), 711–721. <https://doi.org/10.1378/chest.14-3005> (2015).
12. Lawlor, R. T. et al. Prognostic role of high-grade tumor budding in pancreatic ductal adenocarcinoma: A systematic review and meta-analysis with a focus on epithelial to mesenchymal transition. *Cancers (Basel)* <https://doi.org/10.3390/cancers11010113> (2019).

13. Makitie, A. A., Almangush, A., Rodrigo, J. P., Ferlito, A. & Leivo, I. Hallmarks of cancer: Tumor budding as a sign of invasion and metastasis in head and neck cancer. *Head Neck* **41**(10), 3712–3718. <https://doi.org/10.1002/hed.25872> (2019).
14. Voutsadakis, I. A. Prognostic role of tumor budding in breast cancer. *World J. Exp. Med.* **8**(2), 12–17. <https://doi.org/10.5493/wjem.v8.i2.12> (2018).
15. Grigore, A. D., Jolly, M. K., Jia, D., Farach-Carson, M. C. & Levine, H. Tumor Budding: The Name is EMT Partial EMT. *J. Clin. Med.* <https://doi.org/10.3390/jcm5050051> (2016).
16. Lugli, A. et al. Tumour budding in solid cancers. *Nat. Rev. Clin. Oncol.* **18**, 101–115. <https://doi.org/10.1038/s41571-020-0422-y> (2021).
17. Meyer, S. N. et al. Co-expression of cytokeratin and vimentin in colorectal cancer highlights a subset of tumor buds and an atypical cancer-associated stroma. *Hum. Pathol.* **87**, 18–27. <https://doi.org/10.1016/j.humpath.2019.02.002> (2019).
18. Gross, I. et al. The intestine-specific homeobox gene Cdx2 decreases mobility and antagonizes dissemination of colon cancer cells. *Oncogene* **27**(1), 107–115. <https://doi.org/10.1038/sj.onc.1210601> (2008).
19. Zheng, J. et al. Targeted CDX2 expression inhibits aggressive phenotypes of colon cancer cells in vitro and in vivo. *Int. J. Oncol.* **51**(2), 478–488. <https://doi.org/10.3892/ijo.2017.4040> (2017).
20. Yu, J. et al. CDX2 inhibits the proliferation and tumor formation of colon cancer cells by suppressing Wnt/beta-catenin signaling via transactivation of GSK-3beta and Axin2 expression. *Cell. Death Dis.* **10**(1), 26. <https://doi.org/10.1038/s41419-018-1263-9> (2019).
21. Slik, K. et al. CDX2 loss with microsatellite stable phenotype predicts poor clinical outcome in stage II colorectal carcinoma. *Am. J. Surg. Pathol.* **43**(11), 1473–1482. <https://doi.org/10.1097/PAS.0000000000001356> (2019).
22. Bae, J. M., Lee, T. H., Cho, N. Y., Kim, T. Y. & Kang, G. H. Loss of CDX2 expression is associated with poor prognosis in colorectal cancer patients. *World J. Gastroenterol.* **21**(5), 1457–1467. <https://doi.org/10.3748/wjg.v21.i5.1457>. PMID:25663765;PMCID:PMC4316088 (2015).
23. Baba, Y. et al. Relationship of CDX2 loss with molecular features and prognosis in colorectal cancer. *Clin. Cancer Res.* **15**(14), 4665–4673. <https://doi.org/10.1158/1078-0432.CCR-09-0401> (2009).
24. Yu, J. et al. CDX2 inhibits epithelial–mesenchymal transition in colorectal cancer by modulation of Snail expression and β-catenin stabilization via transactivation of PTEN expression. *Br. J. Cancer* **124**, 270–280. <https://doi.org/10.1038/s41416-020-01148-1> (2021).
25. Ranjan, R. A. et al. The chorioallantoic membrane xenograft assay as a reliable model for investigating the biology of breast cancer. *Cancers (Basel.)* **15**(6), 1704. <https://doi.org/10.3390/cancers15061704>. PMID:36980588;PMCID:PMC10046776 (2023).
26. Brabertz, T. et al. Down-regulation of the homeodomain factor Cdx2 in colorectal cancer by collagen type I: an active role for the tumor environment in malignant tumor progression. *Cancer Res.* **64**(19), 6973–7697. <https://doi.org/10.1158/0008-5472.CAN-04-1132> (2004).
27. Gavini, J. et al. Verteporfin-induced lysosomal compartment dysregulation potentiates the effect of sorafenib in hepatocellular carcinoma. *Cell. Death Dis.* **10**, 749. <https://doi.org/10.1038/s41419-019-1989-z> (2019).

Acknowledgements

The Translational Research Unit (TRU) and Deborah Shan-Krauer are gratefully acknowledged for excellent technical support. This study was supported by the Swiss National Science Foundation (31003A_166578 and 310030_197786 to IZ and MPT) and a Swiss Government Excellence Scholarship (ESKAS, nr. 2021.0019 / Kosovo / OP) to RM.

Author contributions

NB, KU, RM and CSD performed experiments and drafted the manuscript. AL and HD scored tumor budding and provided clinical background. DS provided CRC liver metastasis PDX samples and helped with study design. NGTW performed CAM assays. ÖDW, MPT, and IZ designed the study, performed statistical evaluations, wrote, and edited the manuscript. All authors approved the final version of the paper.

Declarations

Competing interests

The authors declare no competing interests.

Additional information

Supplementary Information The online version contains supplementary material available at <https://doi.org/10.1038/s41598-025-07278-x>.

Correspondence and requests for materials should be addressed to I.Z. or M.P.T.

Reprints and permissions information is available at www.nature.com/reprints.

Publisher's note Springer Nature remains neutral with regard to jurisdictional claims in published maps and institutional affiliations.

Open Access This article is licensed under a Creative Commons Attribution 4.0 International License, which permits use, sharing, adaptation, distribution and reproduction in any medium or format, as long as you give appropriate credit to the original author(s) and the source, provide a link to the Creative Commons licence, and indicate if changes were made. The images or other third party material in this article are included in the article's Creative Commons licence, unless indicated otherwise in a credit line to the material. If material is not included in the article's Creative Commons licence and your intended use is not permitted by statutory regulation or exceeds the permitted use, you will need to obtain permission directly from the copyright holder. To view a copy of this licence, visit <http://creativecommons.org/licenses/by/4.0/>.

© The Author(s) 2025